University of Wyoming Aeronautics Laboratory
Mechanical Engineering Department

Jonathan W. Naughton
University of Wyoming Aeronautics Laboratory
Mechanical Engineering Department
College of Engineering
University of Wyoming
PO Box 3295
Laramie, Wyoming 82071
Phone (307)766-6284 FAX (307)766-2695
Email: Naughton@uwyo.edu

UWAL-2002-02

Reduction of Base Drag on Launch Vehicles

Final Report
Jonathan W. Naughton
March, 2000 through March 2002
NASA Research Grant NAG4-208

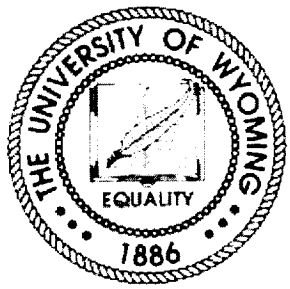

Abstract

Current reentry vehicle designs exhibit large amounts of base drag due to large base areas. These large base areas can arise from the integration of the propulsion system (X-33) or control surface placement (X-38). Large base drag limits the vehicle's cross-range capability and causes a large glide-slope angle. Fortunately, there appears to be a possible means of lowering the base drag on these vehicles. Based on early work on the subsonic aerodynamics of lifting bodies, it appears that the addition of small amounts of viscous fore-body drag can produce a significant reduction in base drag. Recent work suggests that this phenomenon also occurs in the transonic and supersonic flight regimes.

This report summarizes a study designed to demonstrate the reduction of base drag through the addition of fore-body viscous drag. The present study has focused on the measurement of viscous fore-body drag and the demonstration of the relationship between fore-body viscous drag and base drag at Reynolds Numbers up to $2.5x10^6$. The results of the present work do not conclusively demonstrate that viscous fore-body drag reduces base drag. The apparent contradictory results of the present study are attributed to the different geometry used in the present study. However, the results suggest that the increased boundary layer thickness at separation caused by larger fore-body viscous drag somehow affects the vortex structure in the wake thereby reducing the base drag. More research is required to confirm this postulated mechanism.

Introduction

Recent lifting body and wing-body designs for single stage-to-orbit or for crew return from the space station are all derived from variations on the original lifting body concept (Wong 1958). For a variety of reasons, these designs all have large base areas relative to the vehicle size. For example, on the X-33 configuration, the large base areas are required to accommodate aero-spike engines. Conversely, the X-38, derived from the original X-24A mold lines, has a large blunt base area caused by the upper body flap required to trim the vehicle. In both of the above cases, the base area is highly separated resulting in large negative base pressure coefficients. Because of the large base-to-wetted-area ratios of these vehicles, the base drag comprises the majority of the overall vehicle drag. Thus, the base drag has a large impact on critical vehicle performance parameters such as maximum payload and maximum cross-range. Any decrease in base drag has the potential to significantly improve the overall vehicle performance.

Fortunately, there appears to be a feasible means for decreasing base drag. For blunt-based objects whose base areas are heavily separated, a clear relationship between the base drag and the "viscous" fore-body drag has been demonstrated (Hoerner 1965, Saltzman *et al.* 1999). Fig. 1(a) shows that, for subsonic flow conditions, as the fore-body drag is increased, the base drag of the projectile tends to decrease. This base-drag reduction appears to be a result of a modification of the boundary layer at the base of the vehicle. One theory for the observed drag reduction is that the thickened boundary layer acts as a buffer between the high-speed external flow and the separated base flow. The shear layer that develops between the high-speed external flow and the low-energy, separated air in the base region accelerates fluid in the base region thereby reducing the base pressure. As the viscous fore-body drag is increased, the boundary layer thickness at the aft end of the fore body increases, thereby reducing the amount of fluid in the separated base area that is accelerated. Due to the reduction of momentum transfer to the base area, the base pressure coefficient rises resulting in a reduction of base drag.

Whatever the exact cause of the increased base pressures, projectiles whose base drag coefficient is greater than 0.30 (referenced to the base area) have ratios of base drag to viscous fore-body drag that lie on the steep vertical portion of the curves shown in Fig. 1(a). In this region, a small increment in the viscous fore-body drag should result in a relatively large decrease in the base drag. If the added increment in fore-body viscous drag is optimized with respect to the base drag reduction, then it may be possible to reduce the overall drag of the configuration. This optimal drag-region, or "drag bucket," is depicted in figure 1(b). Here an estimate of the total vehicle drag is plotted against the viscous fore-body drag. Data from many

flight vehicles (X-15, M2 -F1, M2 - F2, Shuttle, HL-10, X-24A, X-24B, and the SR-71 LASRE) have been used to verify the relationships in Figure 1 (Saltzman 1999, Whitmore & Moes 1999). Whereas the drag characteristics of most of the previously flown hypersonic shapes lie near or slightly to the right of the drag minimum, those of the LASRE (Model of the X-33) lie far to the left of the drag minimum. The simple model of figure 1(b) is presented only as an illustration of the "drag-bucket" concept. Clearly, the fore-body pressure profile, the presence of induced drag, and localized interference or flow separation drag will likely alter the shape of the "optimal" curve presented in figure 2. The challenge is to determine the fore-body drag value that produces the minimum vehicle drag in a real-world configuration.

Recent work on the LASRE flight program has demonstrated that a reduction in base drag may be accomplished by increasing fore-body drag (Whitmore & Moes 1999). In this study, a portion of the fore body of the LASRE vehicle was roughened to increase the fore-body drag. A decrease of base drag was observed at all Mach numbers (subsonic, transonic and supersonic) validating the application of this drag-reduction technique to transonic and supersonic Mach numbers. Unfortunately, the increase in fore-body drag was greater than the reduction in base drag, and thus no net drag reduction was observed. The increase in fore-body drag was due to both increased pressure drag and increased viscous drag caused by the roughened surface.

Although the data taken during the LASRE flight test was very limited, the results indicate that, over a wide range of Mach number, increasing fore-body drag reduces base drag. The goal here is to demonstrate the maximum base-drag reduction with a minimum increase in fore-body drag.

The results of a collaborative study between NASA-Dryden and the University of Wyoming investigating the feasibility of reducing base drag through boundary layer control on the fore body is reported here. The important result is that, although it appears possible to reduce total vehicle drag by adding viscous fore-body drag (Whitmore *et al.* 2001), the results from the present study are inconclusive. However, the results appear to be consistent with previous work using splitter plates and suggest a drag-reduction method for these blunt-based vehicles.

The remainder of this report is organized as follows. The project goals and results from a companion study are first discussed. Next, a brief description of the test hardware and instrumentation is provided. Boundary layer profiles, shear stress measurements, integrated drag results, and wake survey results are then presented. Finally, the conclusions, ongoing work, and student involvement in the project are discussed.

Project Goals

The goal of this project is to demonstrate the feasibility of using boundary-layer control on a large base area reentry vehicle to reduce the overall vehicle drag. To accomplish this goal, several intermediate steps must be accomplished. First, a means for measuring fore-body viscous drag on smooth and rough surfaces must be demonstrated. Second, a detailed skin friction, surface pressure, and boundary layer surveys must be designed over a range of roughness and base-to-fore-body-area ratios. Using these measurements, the relationship for the viscous fore-body drag $C_{D,fb}$ versus the base drag $C_{D,b}$ must be rigorously established.

Accomplishing these goals should provide enough information to establish that a net drag reduction can be achieved through the addition of viscous fore-body drag. This work will provide the basis for optimizing the means of introducing of additional fore-body drag and implementing it on an actual reentry vehicle.

Results from a Companion Study

A summary of the results of a companion study by Whitmore *et al.* (2001) is reported here. In their study, the effect of fore-body roughness on a blunt-based model was investigated at Reynolds numbers up to 225,000. In these tests, a measurable decrease in base drag was observed for increasing surface roughness. For the conditions tested, an optimum roughness level was determined that produced a

minimum total drag that was ~15% less than the drag on the smooth model. The base drag coefficient at minimum total drag was between 0.225 and 0.275.

The present study was undertaken to investigate the effect of viscous fore-body drag on base drag at an order of magnitude higher Reynolds numbers than those studied by Whitmore *et al.* (2001). This will support the concept of decreasing base drag using viscous fore-body drag at Reynolds numbers closer to those on actual test vehicles.

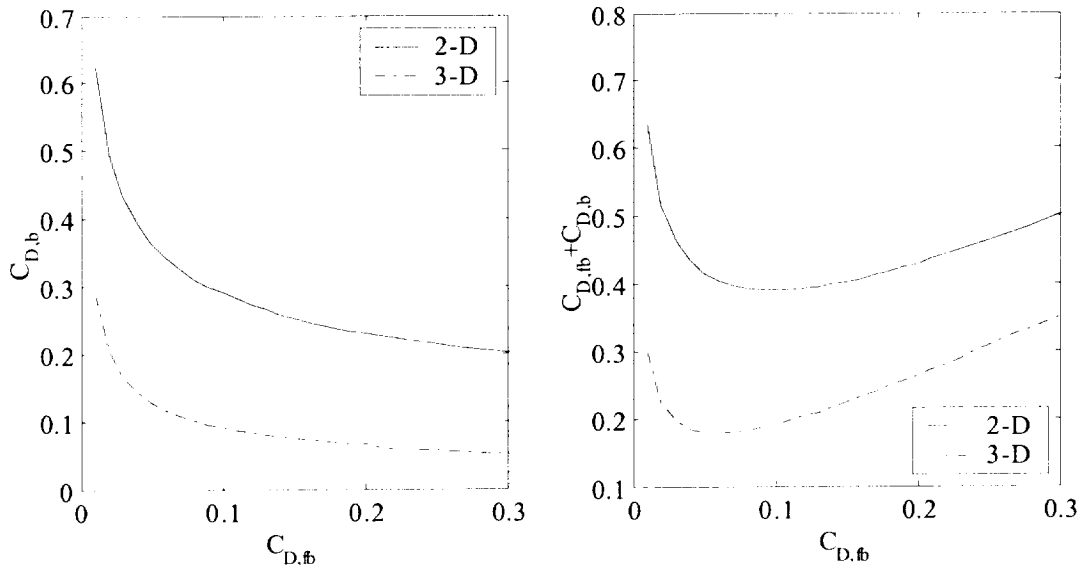

Fig. 1 - Hoerner's relationship between viscous forebody drag and (a) base drag and (b) viscous and base drag for two-dimensional and three-dimensional bodies.

Hardware and Instrumentation

The hardware and instrumentation used in these tests is briefly described below. For details, see Li *et al.* (2001), Li (2001), Decker *et al.* (2002), and Decker (2002).

The tests were carried out in the UWAL 2' × 2' subsonic wind tunnel. This tunnel is an open return wind tunnel with a variable speed fan. The inlet has a 12:1 contraction ratio, and the 2' × 2' × 4' test section has a free-stream turbulence intensity of 3% with the current model installed. The tunnel will run at Reynolds numbers up to 3.0×10^6/m.

The model used in this study is shown in Fig. 2. The ramp was removable such that no ramp (flat plate), a 3° ramp, or a 5° ramp configurations were possible. These ramps provided different base areas but also created favorable pressure gradients of different strengths. Rough surfaces are created using silicon sand glued to the plate using a spray-applied glue. Various sizes of sand grains are used to produce sand-grain roughness values k of 0.25 mm, 0.80 mm, and 1.18 mm. As shown in Fig. 3, the model was equipped with interchangeable plates that included plates with various roughnesses, a stainless plate for oil-film interferometry, and a plate equipped with pressure taps.

To characterize the boundary layers and measure the viscous and pressure drag, pressure measurements, shear stress measurements, and boundary-layer velocity surveys were taken. Hot-wire anemometry was used for boundary-layer and wake surveys. Oil film interferometry was used for shear stress measurements, and pressure surveys were obtained using two 16-channel pressure transducers.

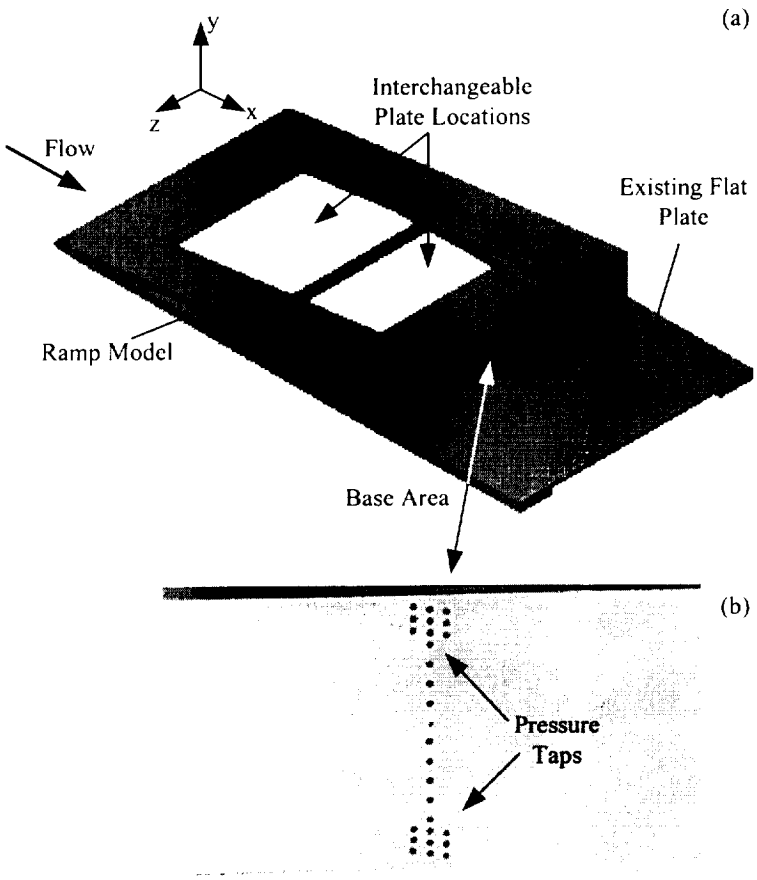

Fig. 2 - Schematic of ramp model used in this study: (a) ramp model and (b) close-up image of the pressure taps in the base region.

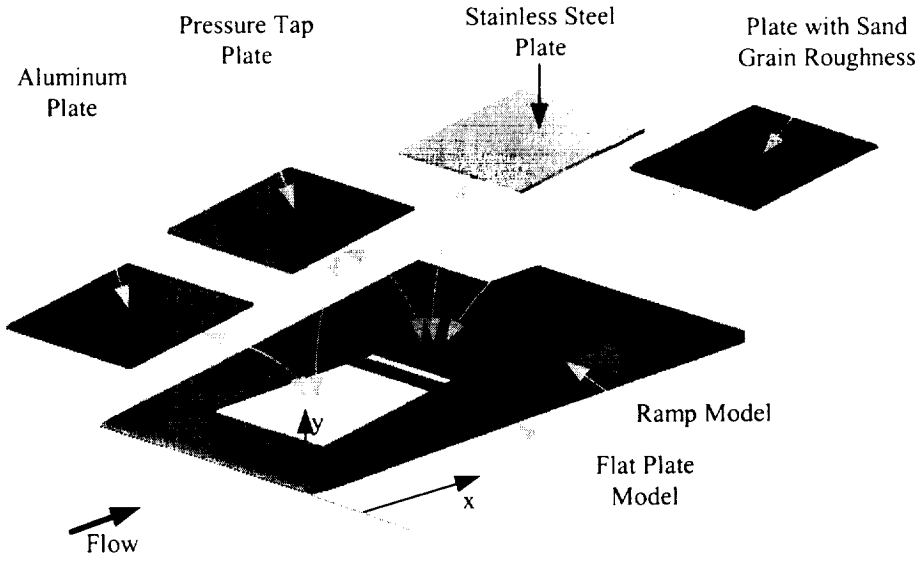

Fig. 3 - Schematic of the ramp model showing the interchangeable plates used in this study.

Results

This study discusses the reduction of base drag on a ramp model by manipulating the boundary layer on the fore body. This work is reported in detail by Li *et al.* (2001), Li (2001) and Decker *et al.* (2002), and Decker (2002), but it is summarized below.

Test Cases

A parametric study has been undertaken to investigate the effects of viscous fore-body drag on base drag. The surface roughness, base height, and pressure gradient are all varied. The Reynolds number is also varied over a small range for the 3° ramp cases to investigate Reynolds number effects (if any) at these high Reynolds numbers. A summary of the cases investigated is provided in Table 1. For each case, the reference velocity U_{ref}, Reynolds number Re_{ref}, ramp angle, and roughness height k are provided. The symbols for the 3° and 5°ramp cases in the table identify these cases in the integrated drag plots shown later. The types of measurements taken for each case are also listed in the table.

Table 1 – Test Cases. The measurements made in each of the cases is listed: HWA – hot-wire boundary layer surveys; OFI – oil-film interferometry skin friction measurements; BP – base pressure measurements; and FB – fore-body pressure measurements. The symbols listed in the table identify each of these cases in the later integrated drag plots.

U_{ref}	Re_{ref} (1/m)	Ramp Angle (deg)	k (mm)	symbol	Measurements
50.0	2.6×10^6	0.0	0.0		HWA, OFI, FBP
50.0	2.6×10^6	0.0	0.25		HWA, OFI, FBP
50.0	2.6×10^6	0.0	0.79		HWA, OFI, FBP
50.0	2.6×10^6	0.0	2.2		HWA, OFI, FBP
30.0	1.5×10^6	3.0	0.0	+	OFI, FBP, BP
40.0	2.0×10^6	3.0	0.0	○	OFI, FBP, BP
47.0	2.3×10^6	3.0	0.0	✱	HWA, BP
47.0	2.3×10^6	3.0	0.25	×	HWA, BP
47.0	2.3×10^6	3.0	0.79	□	HWA, BP
47.0	2.3×10^6	3.0	2.2	◇	HWA, BP
43.0	2.1×10^6	5.0	0.0	▽	HWA, BP
43.0	2.1×10^6	5.0	0.25	▷	HWA, BP
43.0	2.1×10^6	5.0	0.79	◁	HWA, BP
43.0	2.1×10^6	5.0	2.2	★	HWA, BP

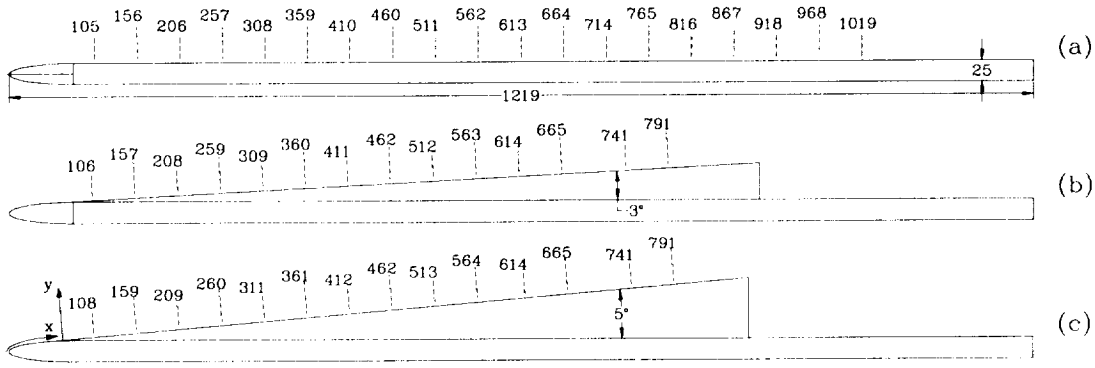

Fig. 4 – Boundary layer survey locations: (a) flat plate; (b) 3° ramp; and (c) 5° ramp.

Boundary Layer Hot-Wire Measurements

The characterization of smooth and rough boundary layers for zero- and favorable pressure gradients has been completed as part of this study. Examination of this data continues due to the unique nature of this data set. This is the first data set of its kind that parametrically investigates the effect of pressure gradient and roughness on a turbulent boundary layer.

A large number of hot-wire surveys on the flat plate with smooth and rough surfaces have been taken. The locations of the surveys on the plate can be seen in Fig. 4(a). Each of the profiles is fit to a composite wall/wake law for rough surfaces (see White (1991) for details on the individual laws and the effects of roughness):

$$u^+ = \frac{1}{\kappa}\ln y^+ + B + \frac{\Delta u}{u_\tau} + \frac{2\Pi}{\kappa}W\left(\frac{y}{\delta}\right),$$

where κ and B are constants, u^+ is the non-dimensional velocity u/u_τ, y^+ is the distance from the wall in wall units yu_τ/ν, u_τ is the friction velocity $\sqrt{\tau_w/\rho}$, $\Delta u/u_\tau$ is the velocity offset due to roughness, Π is the wake strength parameter, and $W(y/\delta)$ is the wake function given by

$$W\left(\frac{y}{\delta}\right) \approx \sin^2\left(\frac{\pi y}{2\delta}\right).$$

To fit the points, a non-linear least squares curve fit is used. Using this curve fit, a preliminary estimate of τ_w can be made. Values of τ_w determined in this way are used to estimate the viscous fore-body drag.

Several surveys near the back of the flat plate plotted in wall coordinates (u^+, y^+) are shown in Fig. 5 for different surface roughness values. In addition to the collapse of the data for each roughness, the effect of increasing roughness is to move the boundary layer profile downward and to the right. This effect is expected of rough boundary layers (White 1991).

In addition to measurements on a flat plate, hot wire measurements have been made in the boundary layer that forms on ramps (See Fig. 4 (b) and (c)). Due to the acceleration of the flow over the ramps, a favorable pressure gradient develops. The ramps are used because, in order to demonstrate the relationship between viscous drag and base drag, a base area is required. This geometry produces a significantly different flow field than a true base flow, but it is a way to test our methods without building an entirely new model. The boundary layer velocity profile on the 3°smooth ramps is compared to the flat plate result in Fig. 6. In this figure, the two profiles collapse onto a single curve with the exception of the wake region. This is the result that is expected for equilibrium boundary layers subject to a pressure gradient, but well

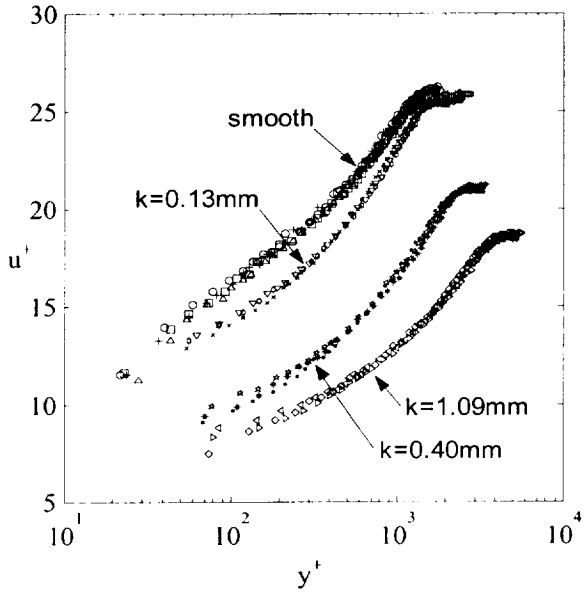

Fig. 5 – Boundary layer surveys on a flat plate for various roughness plotted in wall coordinates. For each roughness, several surveys from have been plotted.

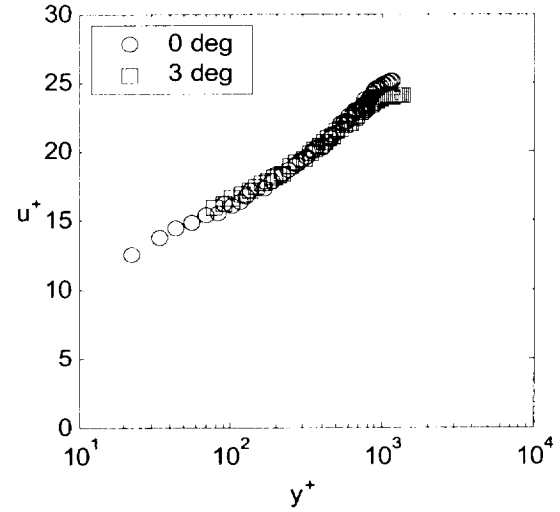

Fig. 6 – Boundary layer surveys on a smooth flat plate and 3° ramp plotted in wall coordinates.

away from separation. The 5° smooth ramp is not shown in this figure because it relaminarizes and cannot be represented by a turbulent boundary layer profile.

Boundary layers subject to both roughness and favorable pressure gradient are expected to produce a boundary layer that contains aspects of both effects. Fig. 7 shows boundary layer profiles for the 3° smooth ramp with several different roughnesses. Several boundary layer profiles near the back of the ramp are shown for each roughness. Fig. 7(a) demonstrates that the smooth 3° ramp results collapse to a single curve as did the smooth flat plate. Fig. 7(b) and (c) show that both the k=0.13mm and 0.40 mm cases fail to collapse to a single curve. However Fig. 7(d) reveals that the k=1.09 mm case again collapses. This suggests that the latter case is fully rough for this pressure gradient, while the intermediate cases are still transitionally rough.

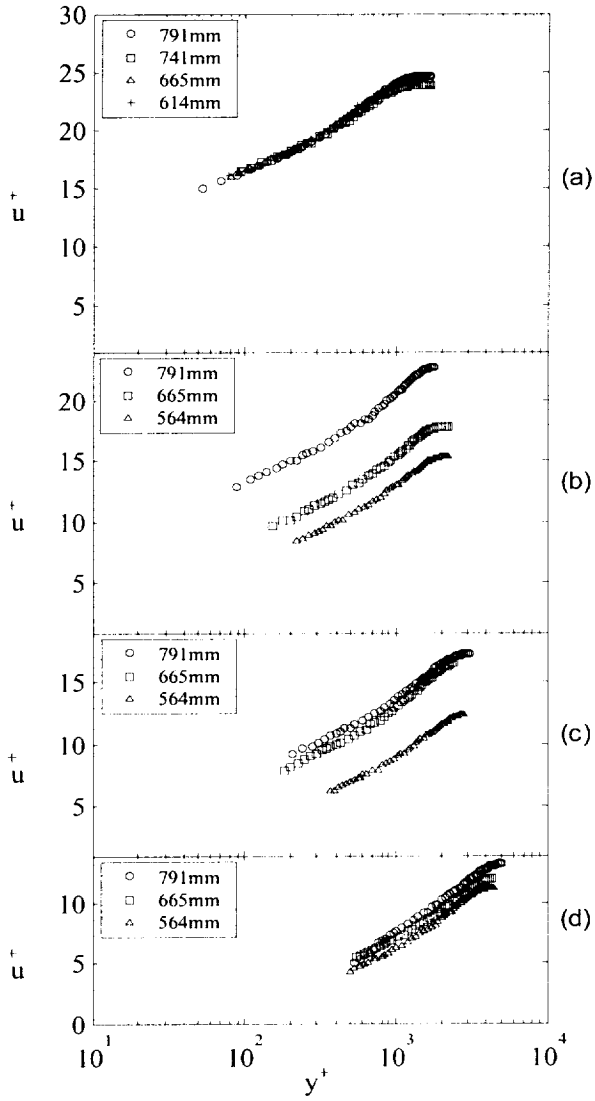

Fig. 7 – Boundary layer surveys on a 3° ramp plotted in wall coordinates for several different roughness values: (a) smooth surface; (b) k=0.25mm; (c) k=0.79mm; and (d) k=2.2 mm.

Estimates of the shear stress distribution determined from velocity profiles are shown in Fig. 8. Several interesting features are evident in this figure. First, the overall trend is that the shear stress increases with both roughness and ramp angle. Second, the shear stress increases by a factor up to 6 when both roughness and favorable pressure gradient are present. Third, the effect of roughness is different depending on the pressure gradient. On the surfaces with a zero pressure gradient boundary layer, the shear stress of the smooth plate and that with the smallest roughness are essentially the same indicating that the smallest sand is hydraulically smooth. When the pressure gradient is increased, the application of the smallest sand increases the shear stress dramatically.

Analysis of these boundary layer surveys continues so that better estimates of the fore-body viscous drag may be obtained. As indicated above, this data set is unique, and preparation of a journal article discussing this data is underway.

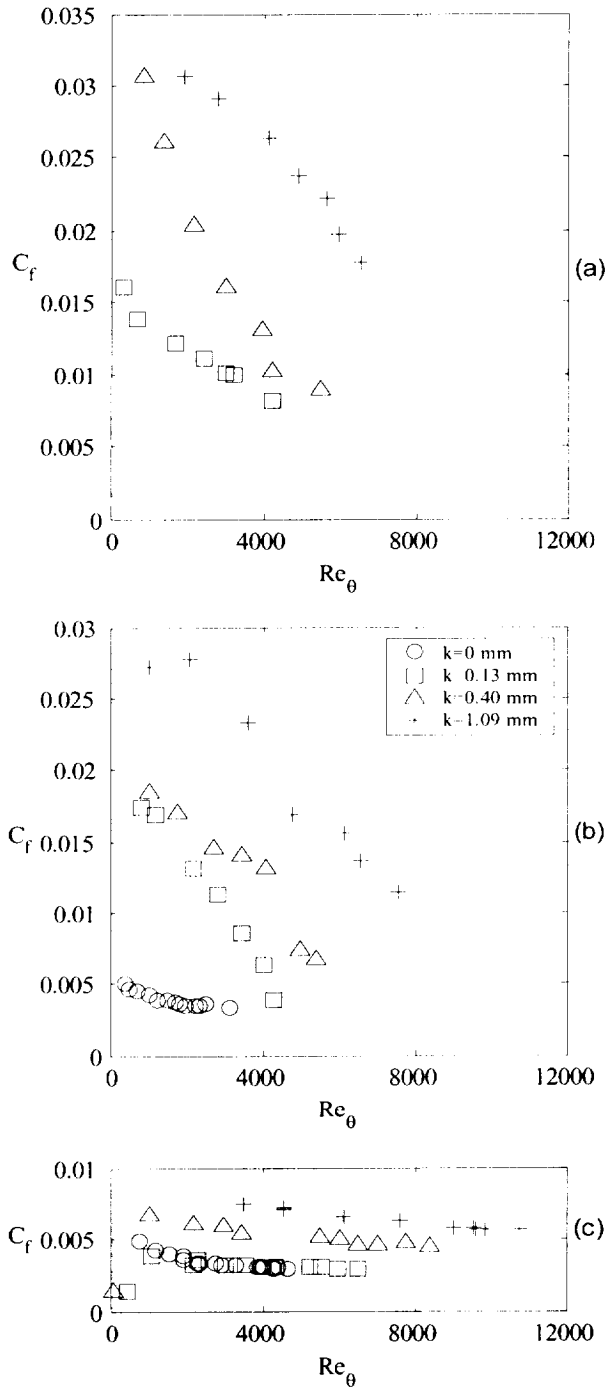

Fig. 8 – Skin-friction coefficient determined from boundary layer surveys: (a) 5° ramp; (b) 3° ramp; and (c) flat plate.

Shear Stress Measurements via Oil-Film Interferometry

Shear stress measurements have been made on the smooth surfaces using oil-film interferometry. These measurements provide a separate measurement of shear stress for the smooth surface cases and

provide a means of evaluating shear stress measurements inferred from velocity measurements in favorable pressure gradients.

The oil film interferometry skin-friction measurement technique will not be discussed here. For a general review of the technique, see Naughton and Sheplak (2000), and for a discussion of its application in this flow see Decker (2002) and Decker *et al.* (2002).

Example results of oil film interferometry measurements from the present study are shown in Fig. 9, where the skin-friction distribution on a smooth flat plate is presented. As can be seen in the figure, the results from the smooth flat plate agree with the theoretical result. Due to their higher accuracy, the measurements of C_f made using oil-film interferometry are used when possible to determine the viscous fore-body drag, since they are more accurate than the values determined using the boundary-layer surveys. This figure also demonstrates that the wall shear stress determined from fitting the boundary layer produces acceptable results for this case.

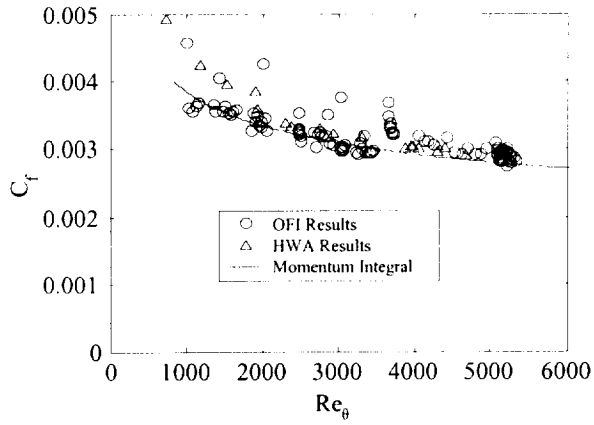

Fig. 9 – Example C_f results from oil-film interferometry measurements.

Base Drag versus Viscous Fore-Body Drag Results

The primary goal of this work is to determine the relationship between viscous fore-body and base drag. In order to evaluate the data acquired in this study with the relationships in Fig. 1, corrections are applied to the data to account for the blockage effect in the wind tunnel. The effect of blockage is to increase the acceleration along the body over what it would be in an unconfined flow. Due to the accuracy required in the present experiment and the large blockage associated with the model, simple blockage correction approaches are not used. Instead, two-dimensional simulations of the flow in the wind tunnel and in an unconfined flow have been carried out, and the ratio of the two simulations is used to correct the pressure and skin friction coefficients. The flows have been simulated using OVERFLOW, a Reynolds-Averaged Navier-Stokes (RANS) solver. For more information about the simulations, see Decker (2002).

Once corrected, the shear stress and pressure coefficients are integrated to determine the viscous fore-body drag and the base drag. Fig. 10 shows the relationship between these two quantities for several different cases. As is evident in this figure, there is little effect on the base drag for all levels of viscous fore-body drag. The two curves shown in the plot are Hoerner's curves for 2-D surface imperfections and 3-D bodies. It appears from this figure that the ramp behaves similarly to a 2-D surface imperfection. This will be discussed further below.

Due to the large pressure gradients on the body even when the pressures are corrected for blockage, the pressure on the fore body just upstream of the base region is much lower than the pressure at the front of the fore body. If this pressure difference is not taken into account, the base drag could appear artificially high. To correct for this result, the drag from the fore body (which is actually a thrust) is added to the base drag in Fig. 11 thus lowering the values on the vertical axis. In essence, the relationship shown in the plot

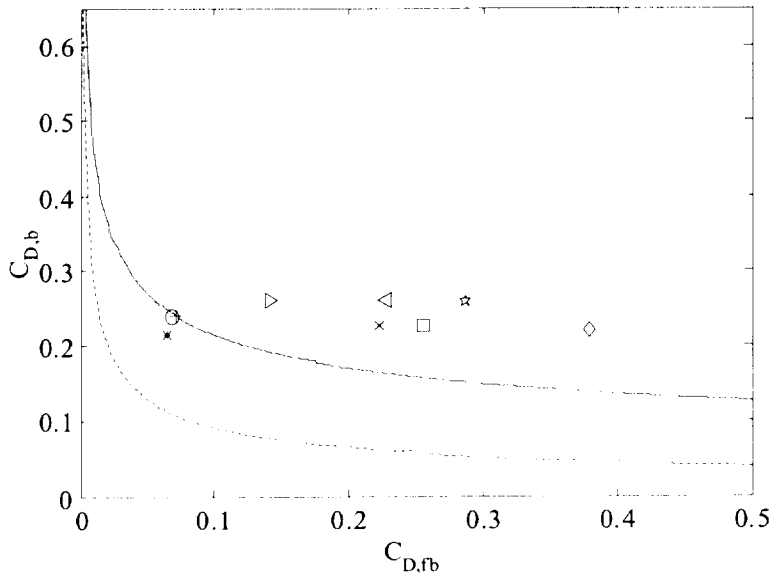

Fig. 10 – Effect of viscous fore-body drag on base drag. Data for several different cases are shown (see Table 1 to identify the cases associated with the different symbols).

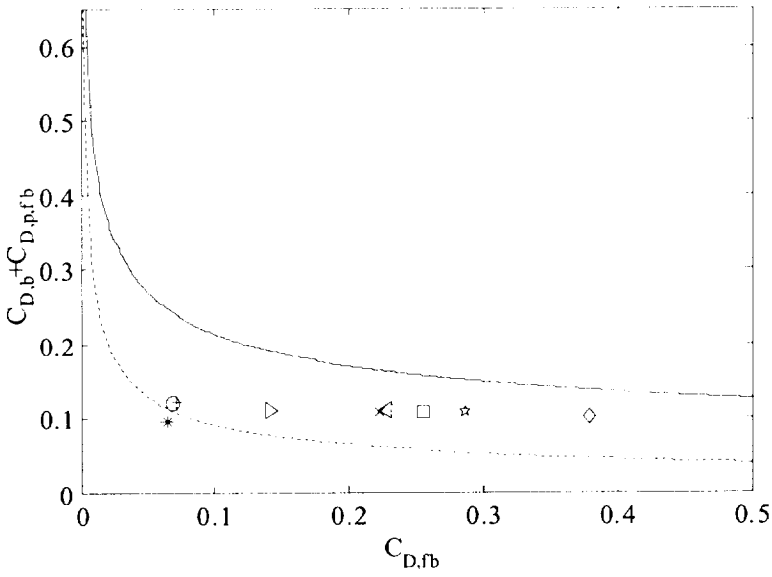

Fig. 11 – Effect of viscous fore-body drag on fore-body and base pressure drag. Data for several different cases are shown (see Table 1 to identify the cases associated with the different symbols).

is now the effect of viscous fore-body drag on pressure drag. The nature of the plot is similar to that in Fig. 10, but the values for all cases now fall between the empirically-derived curves shown.

If the fore-body viscous drag is added to the pressure drag, the total drag may be plotted versus viscous fore-body drag. This relationship, shown in Fig. 12, indicates that all of our cases lie to the right of the drag bucket, which can partially account for the lack of sensitivity of the base drag to viscous fore-body drag.

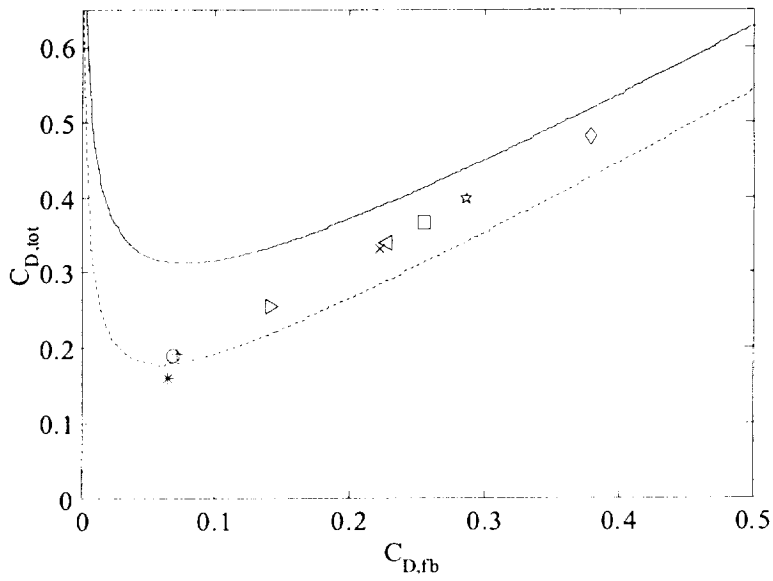

Fig. 12 – Effect of viscous fore-body drag on total drag. Data for several different cases are shown (see Table 1 to identify the cases associated with the different symbols).

The results from this study appear to contradict the relationships developed by Hoerner (1965) and the measurements of Whitmore *et al.* (2001). We believe that the results shown here do not follow the classic two-dimensional result for base flows since the current geometry is actually a ramp with a backward facing step. Thus, the results behave more similarly to the two-dimensional surface imperfection curve shown in Figs. 10 and 11. However, these results indicate that something more complicated than a simple thickening of the boundary layer to reduce acceleration of the base fluid is occurring in actual base flows. If that mechanism were responsible, a similar behavior would be observed in the present case. Instead, we believe that the reduction in base drag observed in actual base flows is linked to a modification of the dynamics of the vortex shedding at the base. Modifying the interaction between the vortex shedding on either side of the base region by mechanisms such as splitter plates has been shown to reduce base drag (see Tanner1975).

Hot-Wire Wake Surveys

To investigate why the base drag is unaffected by the addition of fore-body roughness, hot-wire surveys have been made in the near wake of the ramp base. Although these surveys are not extensive, they suggest that the flow is influenced by the presence of the flat plate downstream of the ramp base area. The flat plate surface here acts like a splitter plate in a base flow and has a large effect on the flow-field in the base area, and thus a large effect on the base pressure and base drag.

Spectra of the measurements just downstream of the base (0.59 base heights) and at a distance above the flat plate approximately equal to the base height are shown in Fig. 13. As is evident in the figure, there is no evidence of a strong periodic component for any roughness value that might be expected in this region of a typical base area. This is likely the cause for the insensitivity of the base pressures to changes in the viscous fore-body drag. Whether the lack of a visible periodic component is a result of the splitter plate or the high values of fore-body viscous drag is not clear at this point.

Conclusions

An extensive parametric study of a ramp with a base area has been carried out. To accomplish this, means of measuring fore-body viscous drag on smooth and rough surfaces have been investigated. These

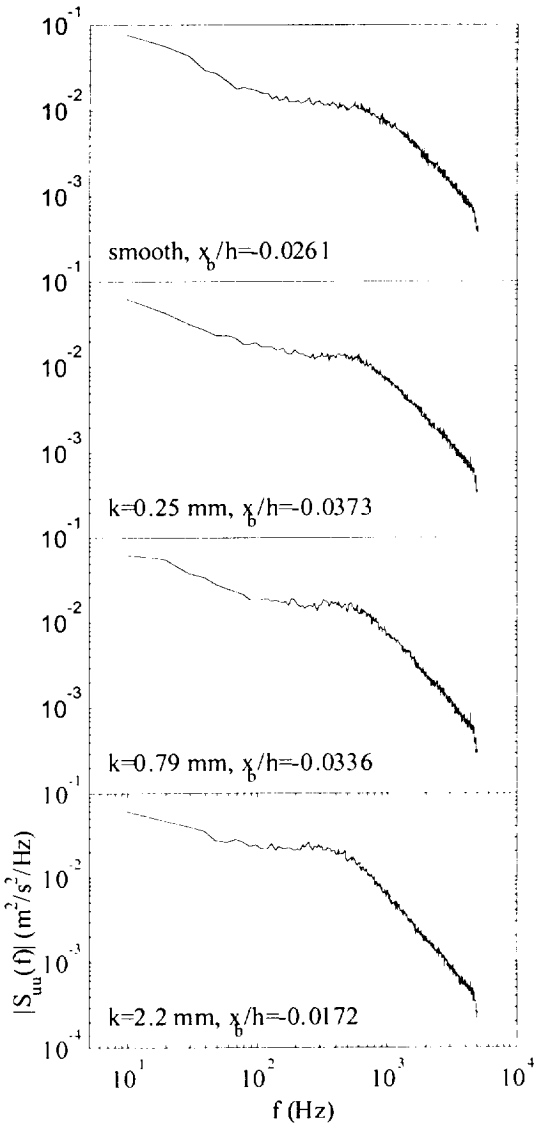

Fig. 13 – Auto-spectral density of the velocity in the wake of the 3° ramp at the step height h and approximately 0.6 step heights downstream of the ramp base.

skin-friction measurement techniques have been used with pressure measurements to determine the relationship between viscous fore-body drag and base drag.

The measurement of viscous drag continues to pose challenges for the aerodynamics community. In the present study, oil-film interferometry has been used to make high-quality shear stress measurements on smooth surfaces. However, boundary-layer surveys have been employed on rough surfaces. These latter measurements have much higher uncertainties due to the difficulty of finding unique fits of the data using a combined wall-wake law for rough surfaces. Research on accurate measurements of skin friction on rough surfaces is a critical area and improved methods for measuring shear stress on rough surfaces are needed.

From this study, it appears clear that the addition of fore body viscous drag to this geometry did little to reduce base drag. This provides indirect proof that, in flows with true base areas (rather than the backward facing step used in this study), the simple explanation that thickening the boundary layer reduces acceleration of the low-momentum base area fluid is invalid. We believe that the thickening of the

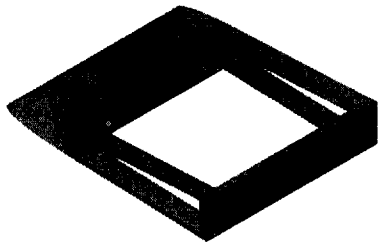

(a)

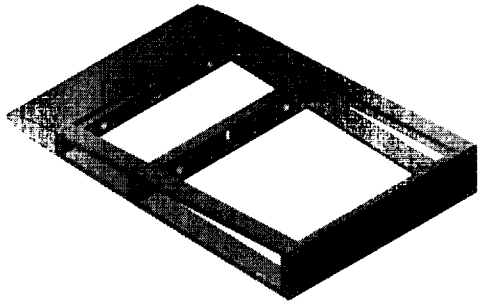

(b)

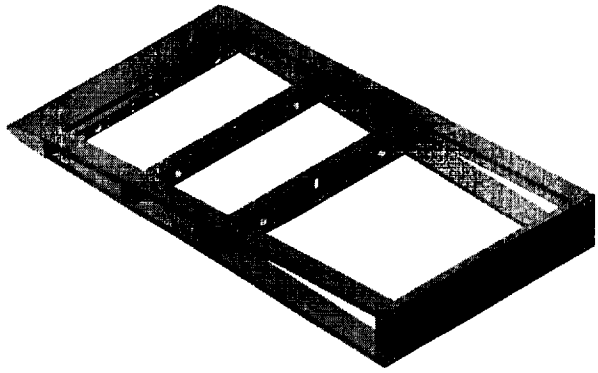

(c)

Fig. 14 – Wedge model with various fore-body areas: (a) one module; (b) two modules, and (c) three modules.

boundary layer must somehow affect the complicated shedding process that occurs in the base area and thereby reduces base drag. Further work must be carried out to conclusively demonstrate this.

A by-product of this work is a set of detailed measurements in a rough turbulent boundary layer in a favorable pressure gradient. This data set is unique and has shown that turbulent boundary layers in favorable pressure gradients are very sensitive to roughness – much more so than their zero-pressure-gradient or favorable-pressure-gradient counterparts.

Ongoing Work

Analysis of the detailed favorable pressure gradient turbulent boundary layer surveys continues. Understanding the results is difficult due to the combined effects of the roughness and pressure gradient. This analysis should be complete soon, and an archival publication of these important results is underway.

In order to conclusively demonstrate the reduction of base drag by adding viscous fore-body drag, a new model is in the final stages of construction and will undergo testing in the near future. This model, shown in Fig. 14, is a simple 2.5° ramp that terminates in a base region. The nose of the body is an ellipse. By extending the fore body forward while maintaining the same base area, an increase in viscous drag can be realized. As shown, the model has three separate configurations that can double the base area. In this way, the model can be used to determine which of the three configurations is closest to the "drag bucket," and then the fore-body viscous drag on that configuration can be varied in small amounts by using surface roughness. This model will undergo tests in late summer and fall 2002.

Student Involvement

Students were involved in all aspects of this work. Two students, Weixia Li and Robert Decker, received their Master's degrees as part of this work. Both of these students presented their work at an AIAA technical meeting. In addition, several undergraduates were involved with various aspects of the work presented here.

References

General

1. Hoerner, S.F., *Fluid Dynamic Drag*, Self-Published Work, Library of Congress Card no. 64-1966, Washington, DC, 1965, pp. 3-19, 3-20, 15-4, 16-5.
2. Naughton, J.W. and Sheplak, M., "Modern Skin Friction Measurement Techniques: Description, Use, and What to do with the Data," AIAA Paper 2000-2521, 21st AIAA Advanced Measurement Technology and Ground Testing Conference, Denver, CO, June 2000.
3. Saltzman, E.J., Wang, K.C., and Iliff, K.W., "Flight-Determined Subsonic Lift and Drag Characteristics of Seven Lifting-Body and Wing-Body Reentry Vehicle Configurations with Truncated bases," AIAA Paper 99-0383, 37th AIAA Aerospace Sciences Meeting, Reno, NV, January 1999.
4. Tanner, M., "Reduction of Base Drag," *Progress in Aerospace Sciences*, 16(4), 1975, pp. 369—384.
5. Whitmore, S.A., and Moes, T.R.,"A Base Drag Reduction Experiment on the X-33 Linear Aerospike SR-71 Experiment (LASRE) Flight Program," AIAA Paper 99-0277, 37th AIAA Aerospace Sciences Meeting, Reno, NV, January 1999.
6. Whitmore, S.A., Sprague, S., and Naughton, J.W., "Wind-Tunnel Investigations of Blunt-Body Drag Reduction Using Forebody Surface Roughness," AIAA Paper 2001-0252, 39th AIAA Aerospace Sciences Meeting, Reno, NV, January 2001 (Also NASA TM-2001-210390). This paper has been accepted for publication in *AIAA Journal of Spacecraft and Rockets*.
7. Wong, T.J., Hermach, C.A., Reller, J.O. Jr., and Tinling, B.E., "Preliminary Studies of Manned Satellites – Wingless Configurations: Lifting Body," NACA Conference on High-Speed Aerodynamics: A compilation of Papers Presented, NASA TM-X-67369, 1958, pp. 35-44.
8. White, F., *Viscous Flow*, McGraw-Hill, 2nd edition, 1991.

Publications from this Work

1. Li, W., Decker, R., Lew, J., Naughton, J., and Whitmore, S., "Characteristics of Turbulent Boundary Layers Rough Surfaces with Favorable Pressure Gradients," AIAA Paper 2001-2915, 31st AIAA Fluid Dynamics Conference, Anaheim, CA, June 2001.
2. Li, W., "Characteristics of Turbulent Boundary Layers on Rough Surfaces with Favorable Pressure Gradients," M.S. Thesis, Mechanical Engineering Department, University of Wyoming, August 2001.
3. Decker, R., Naughton, J., and Jafari, F., "Automatic Fringe Detection for Oil-Film Interferometric Skin-Friction Measurement," in I. Grant and G. Carlomagno, editors, Proceedings of the 9th International Symposium on Flow Visualization, 2000 (On CD ROM, ISBN 0 953391 1 7).
4. Decker, R., Naughton, J., and Whitmore, S., "Modification of Base Drag through Boundary Layer Manipulation," AIAA Paper 2002-0273, 40th AIAA Aerospace Sciences Meeting, Reno, NV, January 2002.
5. Decker, R., "Viscous Drag Measurements and its Application to base Drag Reduction", M.S. Thesis, Mechanical Engineering Department, University of Wyoming, May 2002.